Quantum Cascade Lasers without Intersubband Population Inversion

Jerôme Faist, Federico Capasso, Carlo Sirtori, Deborah L. Sivco, Albert L. Hutchinson, Mark S. Hybertsen, and Alfred Y. Cho

AT&T Bell Laboratories, Murray Hill, New Jersey 07974-0636

(Received 20 June 1995)

The fundamental limits of the operation of quantum cascade intersubband lasers are investigated. Band nonparabolicities combined with the nonthermal electron distribution in the active region make laser action possible even in the absence of global k-space population inversion between subbands, i.e., when the lifetime of the lower subband exceeds that of the upper one. A laser based on local k-space population inversion with single-quantum-well active regions is demonstrated and its performance compared to that of quantum cascade lasers with double-quantum-well active regions.

PACS numbers: 42.55.Px, 73.40.Gk, 78.60.–b, 78.66.–w

Recently, a semiconductor laser [quantum cascade (QC) laser] based on unipolar injection and intersubband emission was demonstrated [1–3]. In the original report [1], we stressed that when band nonparabolicities are negligible-intersubband optical transitions are characterized by an "atomiclike" joint density of states and that as a result QC lasers bear strong similarities with the so-called four-level lasers typical of many gaseous and solid-state media. In this Letter, we probe the important role of energy dispersion in the plane of the layers and of intrasubband electron relaxation kinetics in the operation of QC lasers.

In the QC laser [Fig. 1(a)] the anticrossing between the two low energy states ($n = 0$ and $n = 1$) of the double-well active region is engineered so that their energy difference under the bias conditions required for injection into the $n = 2$ state is resonant with the optical phonon energy [1]. This ensures an ultrashort intersubband scattering time ($\tau_{10} \leq 0.6$ ps) between the $n = 0$ and $n = 1$ states due to the zero momentum transfer [1–3]. On the other hand, the intersubband scattering time between excited states 2 and 1 is significantly longer ($\cong 1.8$ ps) owing to the much greater momentum transfer associated with the large energy separation between the two subbands ($\sim$300 meV). This favorable ratio of times ensures global (i.e., integrated over the electron wave number) population inversion but, as we show below, is not a necessary condition for lasing in intersubband lasers. To clarify this important point we shall consider a simpler structure [Fig. 1(b)] with *single-well* active regions replacing the double-well ones of Fig. 1(a). Here electrons are tunnel injected into the first excited state of a GaInAs quantum well. The superlattice of the injector-relaxation region in both structures is designed as a Bragg reflector to suppress the escape of electrons from the $n = 2$ excited state of the quantum well into the continuum while allowing their extraction from the lower state ($n = 1$) of the well [3]. Since the single quantum well and our double quantum well have by design very similar upper state lifetimes and oscillator strengths, and the electron injectors and optical waveguides have identical designs, *differences in the gain coefficient between the two structures can solely arise from a different distribution of the electron population in the lower state of the lasing transition.*

Figure 2 shows the dispersion of the $n = 1$ and $n = 2$ subbands of the 4.8 nm quantum well of the QC laser of Fig. 1(b), as calculated from an eight-band k^*p model [4]. Note the large energy differences ($\Delta E = 70$ meV) between photons emitted at or near $k = 0$ and the ones absorbed by electrons at large k after having undergone optical phonon scattering from the upper subband. This is due to the bulk band nonparabolicity. The measured spontaneous emission spectrum peaks at an energy corresponding to the intersubband separation at $k = 0$, and its full width at half maximum ($\cong 13$ meV) is significantly smaller than ΔE. As such it does not overlap in energy with the absorption spectrum of electrons that have emitted up to six optical phonons after scattering from the $n = 2$ to the $n = 1$ subband. It follows that for laser action to take place it is sufficient to obtain *local* population inversion in a small region of k space near $k = 0$ corresponding to electron energies within an optical phonon ($\sim$34 meV) from the bottom of the lower subband. This is easier to achieve than in the absence of nonparabolicities (effective four-level system) since only a fraction of the lower subband population contributes to absorption. In our undoped active regions, energy relaxation of the electron distribution in the lower subband ($n = 1$) is dominated by the emission of optical phonons at the low temperatures of our experiments. This gives rise to a characteristic nonthermal electron distribution with phonon replica [5] observed experimentally [6]. Energy loss through electron-electron interaction between the active region and the doped graded gap injector is negligible due to the spatial separation (30 nm) of the two regions and the large energy difference ($\sim$0.3 eV) between the $n = 2$ state and the conduction band edge in the relaxation region. Note that electron-electron scattering within the distribution in the lower subband is estimated to occur in a time scale (>200 fs, Ref. [7]) greater than the intrasubband scattering time by emission of optical phonons

and will merely induce a broadening of the electron distribution significantly smaller than the optical phonon energy. We assume that the emission of the latter is controlled by quasimonochromatic longitudinal phonons with an energy equal to that of the GaAs-like mode in InGaAs ($\hbar\omega_{\mathrm{LO}} = 34$ meV) [8]. This is a reasonable approximation in light of the weak electron-phonon coupling with the InAs-like mode [8]. For the upper subband ($n = 2$) instead, electrons are in a thermal distribution near the lattice temperature since they are resonantly injected near $k = 0$, and the intersubband Auger scattering rate is negligible ($\tau^{-1} \sim 0.2$ ns^{-1}, Ref. [9])

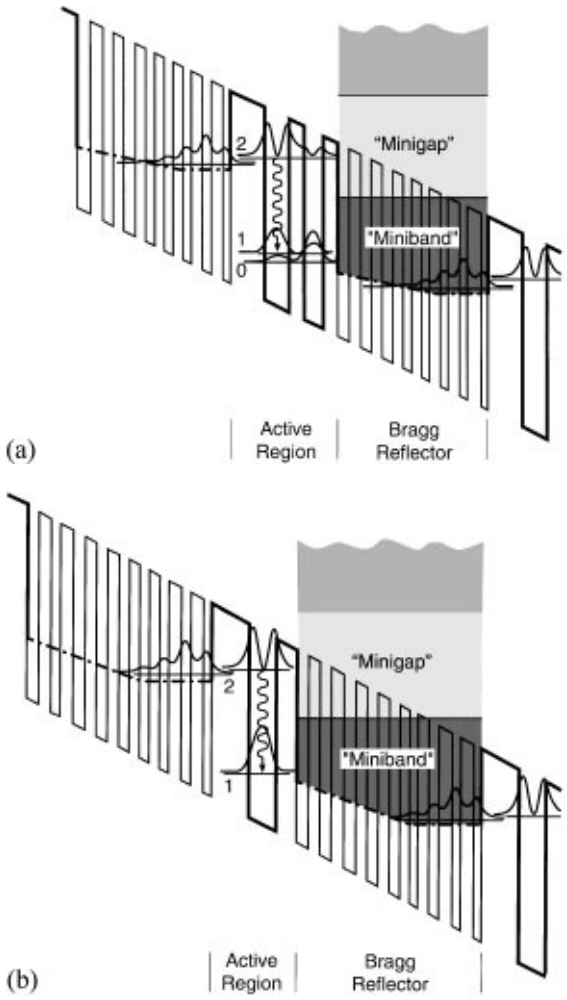

FIG. 1. Schematic conduction band diagram of a portion of the double-quantum-well (a) and single-quantum-well (b) structures under positive bias condition (70 kV/cm). The dashed lines are the effective conduction band edges of the superlattice graded gap electron injector-relaxation regions. The area denoted as "miniband" represents the energy range and spatial extension of bandlike states. As shown, this superlattice is also designed to create a "minigap" that blocks electron escape from level 2. The wavy lines indicate the transitions responsible for laser action. The moduli squared of the relevant wave functions are shown. The $Al_{0.48}In_{0.52}As/Ga_{0.47}In_{0.53}As$ layer sequence, in nanometers, from left to right and starting from the injection barrier is (6.8/4.8), (**2.8**/**3.9**), (**2.7**/2.2), (2.2/2.1), (2.1/2.0), (2.0/1.8), (1.8/1.7), (2.0/1.6), (2.2/1.6), (2.4/1.4) for the structure of (a) and (6.8/4.8), (**3.5**/**2.3**), (**1.9**/2.2), (2.2/2.1), (2.1/2.0), (2.0/1.8), (1.8/1.7), (2.0/1.6), (2.2/1.6), (2.4/1.4) for that of (b). The structure is left undoped, with the exception of layers number twelve through eighteen which are n-type doped to $\cong 3 \times 10^{17}$ cm^{-3}.

We divide all electrons that have scattered down from the $n = 2$ into the $n = 1$ subband into an energy ladder with N (= 7) steps of width equal to $\hbar\omega_{\mathrm{LO}}$ [5]. We can then write rate equations for the number of electrons in each step i and for the number of electrons injected by resonant tunneling into the higher subband near $k = 0$. The resulting $N + 1$ equations contain the tunneling escape rate $(\tau_{\mathrm{tu}})^{-1}$ from the $n = 1$ subband, the lifetime τ_2 of the $n = 2$ state which is determined, to a good approximation by the intersubband optical phonon scattering rate [10], i.e., $\tau_2 \cong \tau_{21} = 1.4$ ps, and the intrasubband scattering rates $(\tau_{\mathrm{int},i})^{-1}$ [10]. For $i = 7$, corresponding to an electron with large kinetic energy parallel to the layers, the calculated intrasubband scattering time $\tau_{\mathrm{int},7}$ is 0.20 ps; it decreases with the electron energy and is 0.12 ps for $i = 1$, i.e., for an electron with an in-plane energy just above $\hbar\omega_{\mathrm{LO}}$ in the lower subband. In steady state one finds that in order to have population inversion between electronic states in the two subbands within $\hbar\omega_{\mathrm{LO}}$ from $k = 0$, the following condition must be satisfied:

$$\tau_{21} > \tau_{\mathrm{tu}} \prod_{i=1}^{7} \frac{\tau_{\mathrm{tu}}}{\tau_{\mathrm{int},i} + \tau_{\mathrm{tu}}} . \qquad (1)$$

The product in Eq. (1) represents the probability that an electron scattering from the upper subband relaxes to the bottom of the lower subband. Figure 2 illustrates pictorially one of such cascade processes. Thus even if the lifetime of the lower excited state (τ_{tu}) is longer than that of the upper one (τ_{21}), one can obtain population inversion. Because of the finite coherence length λ_{coh} in the graded superlattice region [2] ($\lambda_{\mathrm{coh}} \sim$ 2–3 periods), the tunneling escape time out of the $n = 1$ state across the effective barrier created by the 3.5 nm AlInAs layer and the first two periods of the superlattice is $\tau_{\mathrm{tu}} \sim$ 2–3 ps.

Two laser structures were grown with single-well and double-well active regions, respectively. The wavelength core of the first structure comprises $N_p = 25$ active regions alternated with digitally graded superlattice injection-relaxation regions according to the design (thickness and doping levels) discussed in the caption of Fig. 1. The second structure has $N_p = 25$ double-well active regions [Fig. 1(a)] separated by superlattice Bragg reflector injection-relaxation sections identical to the ones of the single-well active region structure. The waveguides in the two structures are identical and incorporate an AlInAs layer and the InP substrate for the upper and lower claddings, respectively [3,11].

The samples were measured in pulsed mode (50 ns width with a repetition rate of 20 kHz) at low temperature [1–3]. Figure 3 displays the peak optical power P versus drive current I at 10 K for two devices processed with identical length (2.25 mm) and width (11 μm). The

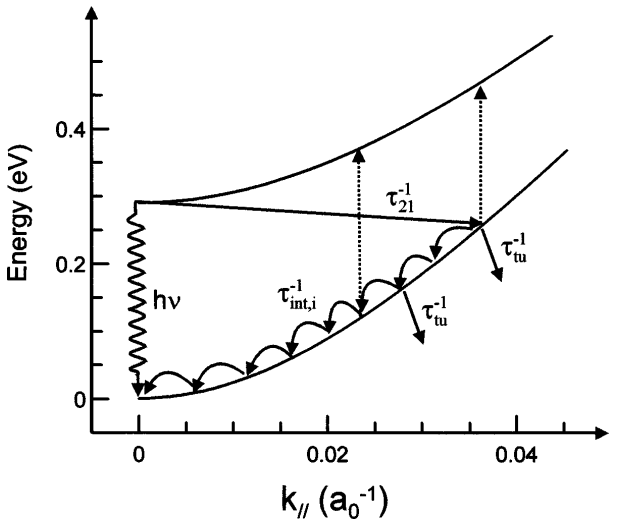

FIG. 2. Calculated dispersion of the two subbands in the 4.8 nm quantum well of the quantum cascade laser of Fig. 1(b); (only positive wave-number states are shown). The wave number parallel to the layers $k_{\|}$ is expressed in units of reciprocal Bohr radius a_0^{-1}. Because of the nonparabolicity, electrons scattered by an optical phonon to the lower subband reabsorb at an energy (vertical dashed arrow) very different (70 meV) from the center ($k = 0$) of the gain curve. One of the many possible electron relaxation routes, by emission of optical phonons, to the bottom of the lower subband is shown.

single-well active layer structure has a threshold current density of 4.5 kA/cm^2 and a slope efficiency dP/dI above threshold (which is proportional to the differential efficiency) of 36 mW/A, whereas for the double-well active region device $J_{\rm th} = 2$ kA/cm^2 and $dP/dI =$ 100 mW/A. These differences are related to the effective removal of electrons from the final state of the laser transition in the case of the double-well active region device due to resonant optical phonon emission, as opposed to the single-well active region laser. Great care was taken to ensure that the results presented in Fig. 3 were genuine characteristics of the design and not by-products of fluctuations in the growth or in the processing. Many devices (~5–10) of each single-quantum-well structure and double-quantum-well structure were tested. Moreover, each growth was duplicated and the results again checked. Fluctuations are within ±10% for the threshold densities and ±15% for the slope efficiencies.

By solving the rate equations and equating the gain to the sum of the waveguide and mirror losses ($\alpha_w + \alpha_m$), one obtains

$$J_{\rm th} = \begin{cases} \frac{A}{\eta_i \tau_2} \frac{\alpha_w + \alpha_m}{1 - \eta \tau_{\rm tu}/\tau_2} & [\text{single well (SW)}], \quad (2) \\ \frac{A}{\eta_i \tau_2} \frac{\alpha_w + \alpha_m}{1 - \eta' \tau_{10}/\tau_{21}} & [\text{double well (DW)}], \quad (3) \end{cases}$$

where η_i is the injection efficiency and

$$A = \varepsilon_0 n_{\rm eff} L_p \lambda (2\gamma)/4\pi q |z_{21}|^2 \Gamma . \quad (4)$$

In Eq. (4), λ (~4.5 μm) is the laser wavelength, 2γ (= 13 meV) is the full width at half maximum of the luminescence, z_{12} (= 1.4 nm) is the dipole matrix element, Γ (= 0.52) is the confinement factor, $n_{\rm eff}$ (= 3.2) is the mode refractive index, L_p (= 50 nm) is the length of the period, ε_0 is the vacuum permittivity, and q is the electron charge. These parameters have all nearly the same values in the two structures so that $A \cong A'$ (within 10%).

Similarly for the differential efficiencies (per facet) above threshold one finds [12]

$$\eta_d = \begin{cases} \frac{N_p \eta_{\rm in}}{2} \frac{\alpha_m}{\alpha_m + \alpha_w} \frac{1 - \eta \tau_{\rm tu}/\tau_2}{1 + (1-\eta)\tau_{\rm tu}/\tau_2} & (\text{SW}), \quad (5) \\ \frac{N_p \eta_{\rm in}}{2} \frac{\alpha_m}{\alpha_m + \alpha_w} \frac{1 - \eta' \tau_{10}/\tau_{21}}{1 + \tau_{10}/\tau_2 - \eta' \tau_{10}/\tau_{21}} & (\text{DW}) . \quad (6) \end{cases}$$

The factor η is equal to the product of branching ratios in Eq. (1); the expression for η' is identical with τ_{10} replacing $\tau_{\rm tu}$. It represents the probability that an electron, after scattering from the $n = 2$ to the $n = 1$ subband, relaxes to the bottom of the latter, without scattering to the $n = 0$ subband. Its small value (0.15) ensures that in the double-well structure the population of the $n = 1$ subband within $\hbar\omega_{\rm LO}$ from $k = 0$ can be neglected with good approximation so that the threshold is inversely proportional to the lifetime of the $n = 2$ state, $\tau_2 = (\tau_{21}^{-1} + \tau_{20}^{-1})^{-1} = 1.25$ ps. Note that the denominator of Eqs. (2) and (3) gives the population inversion condition. The tunneling escape time out of the $n = 0$ state does not appear in Eqs. (3) and (6) since its value is of the order of τ_{10} due to the thin (27 nm) exit barrier; furthermore, only a small fraction (<10%) of the electrons that have scattered from the $n = 1$ to the $n = 0$ state relax to the bottom of this subband before tunneling our of the active region.

The mirror loss ($\alpha_m \cong 6$ cm^{-1}) and the waveguide loss ($\alpha_w \cong 12$ cm^{-1}), obtained from a standard analysis of the measured subthreshold gain spectrum [11], are also essentially the same by design; the injection efficiency η_i, although not known and difficult to calculate, is assumed the same in the two structures since the injection barriers and the bias conditions for injection are the same by design. The internal quantum efficiency $\eta_{\rm in}$ is also assumed the same in the two lasers since it depends primarily on the injection efficiency. We can therefore extract useful physical information from the ratios of thresholds and of slope efficiencies for the two lasers.

Taking the ratio of Eqs. (2) and (3) and equating it to the measured threshold ratio of 2 one obtains for the tunneling escape time $\tau_{\rm tu} = 1.7$ ps. Inserting this value into the ratio of Eqs. (5) and (6) allows us to predict that the coupled well structure should have a slope efficiency a factor of 2.9 higher than the single-well active region structure. This value is in good agreement with the measured ratio of slope efficiencies (= 2.8) thus giving strong evidence that we have realized a quantum cascade laser with an upper state lifetime (τ_2) shorter than that of the lower state ($\tau_{\rm tu}$). From the above value of ($\tau_{\rm tu}$) one finds $\eta = 0.5$. This value, which is significantly larger than η', implies that the population of the

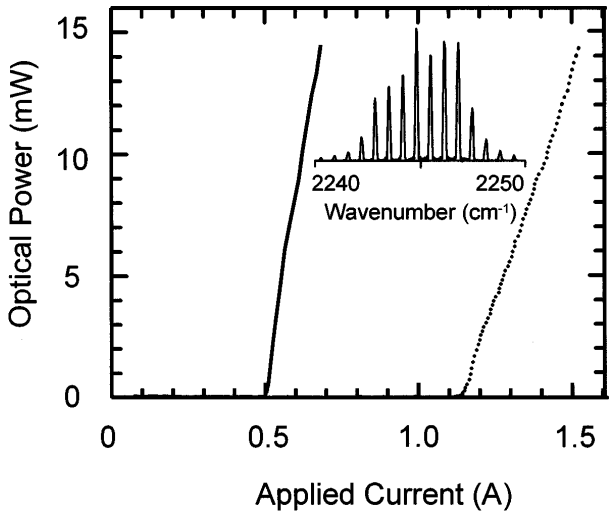

FIG. 3. Peak optical output power from a single facet versus injection current at a heat sink temperature 10 K for the double-quantum-well (solid line) and the single-quantum-well active region laser (dotted line). Inset: high-resolution spectra of the single-quantum-well active laser above threshold.

lower state of the laser transition cannot be neglected in the structure with a single-well active layer. At threshold, we estimate [13] the excited state population to be $n_2 = 2 \times 10^{10}$ cm^{-2} and the total ground state population $n_1 = 2.3 \times 10^{10}$ cm^{-2}, from which the fraction at $k = 0$ is $n_1(k = 0) = 1.15 \times 10^{10}$ cm^{-2}. This is responsible for the higher threshold and smaller differential efficiency compared to the double-well structure. We attribute the difference between the experimental (1.7 ps) and theoretical (2–3 ps) values of the escape tunneling time to additional scattering such as interface roughness scattering. The value derived for τ_{tu} is fixed by the computed intersubband τ_i and intrasubband $\tau_{\mathrm{int},j}$ phonon scattering times. The claim of lack of global population inversion does not depend critically on the choice of these parameters. For example, substituting $\tau_{\mathrm{int},j}$ for an experimental [14] value of 200 fs yields a slightly longer tunneling time $\tau_{\mathrm{tu}} = 1.85$ ps.

The inset of Fig. 3 shows the spectrum of the single-well active region laser at 10 K. Multimode emission is observed, and the modes are separated by the calculated amount $(2n_{\mathrm{eff}}L)^{-1} = 0.62$ cm^{-1}. This laser operated up to 160 K heat sink temperature with a weak temperature dependence of threshold as expected for an intersubband laser [2,3]. The spectrum of the double-well active region laser is instead nearly single mode, similar to that reported previously [3], due to the significantly lower operating current. This device also operated pulsed up to 220 K and continuous wave up to 50 K with 2 mW of power [11]. This better temperature performance than the single-well active region device is largely due to the fact that the $n = 1$ state remains essentially empty in a wide temperature range.

[1] J. Faist, F. Capasso, D. L. Sivco, A. L. Hutchinson, and A. Y. Cho, Science **264**, 553 (1994). For recent proposals on intersubband lasers, Z. Moussa, P. Boucaud, F. H. Julien, Y. Lavon, A. Sa'ar, V. Berger, J. Nagle, and N. Coron, Electron Lett. **31**, 912 (1995); G. N. Henderson, L. C. West, T. K. Gaylord, C. W. Roberts, E. N. Glytsis, and M. T. Asom, Appl. Phys. Lett. **62**, 1432 (1993); G. Sun and J. B. Khurgin, IEEE J. Quantum Electron. **29**, 1104 (1993).

[2] J. Faist, F. Capasso, D. L. Sivco, A. L. Hutchinson, C. Sirtori, S. N. G. Chu, and A. Y. Cho, Appl. Phys. Lett. **65**, 2901 (1994).

[3] J. Faist, F. Capasso, C. Sirtori, D. L. Sivco, A. L. Hutchinson, and A. Y. Cho, Appl. Phys. Lett. **66**, 538 (1995).

[4] For the material and band-structure parameters of GaInAs, see M. S. Hybertsen *et al.*, SPIE Proceedings Vol. 2399 (SPIE-International Society Optical Engineering, Bellingham, WA, 1995), p. 132. The values used for AlInAs are spin-orbit splitting $= 0.325$ eV; Kane energy $E_p =$ 21.7 eV; Luttinger's parameters $g_1 = 9.20$, $g_2 = 3.50$, $g_3 = 4.05$; electron effective mass $= 0.076m_0$; and band gap $= 1.51$ eV. The heterojunction conduction band discontinuity is 0.52 eV. The calculation was done assuming zero applied electric field, since the electric field applied normal to the layers has a negligible effect on the subband dispersion.

[5] A. Grinberg and S. Luryi, Phys. Rev. Lett. **65**, 1251 (1990).

[6] For a review, see S. A. Lyon and C. L. Petersen, Semicond. Sci. Technol. **7**, 821 (1992).

[7] *Hot Carriers in Semiconductor Nanostructures*, edited by J. Shah (Academic Press, San Diego, 1992), p. 212. This time is the one needed to broaden the electron distribution by about 20 meV. Note that our scattering time should be longer since in our case holes are absent, in contrast to the work cited here.

[8] K. J. Nash, M. S. Skolnik, and S. J. Bass, Semicond. Sci. Technol. **2**, 329 (1987).

[9] S. Borenstein and J. Katz, Phys. Rev. B **39**, 10 852 (1989).

[10] P. J. Price, Ann. Phys. (N.Y.) **133**, 217 (1981).

[11] J. Faist, F. Capasso, C. Sirtori, D. L. Sivco, A. L. Hutchinson, and A. Y. Cho, Appl. Phys. Lett. **67**, 3057 (1995).

[12] The expression given in Ref. [3] for the threshold and differential efficiency of QC lasers with vertical transition [Fig. 1(a)] are different since they neglect the effects considered in this paper.

[13] We assume in this calculation an injection efficiency $\eta_{\mathrm{inj}} = 50\%$ which accounts for the observed threshold.

[14] See Ref. [7], p. 367.